A single simulation gives us the SFD for a given size of the parent body and several parameters of the impactor. However, if one wishes to derive the size of the parent body and impactor parameters from the observed SFD, it is necessary to conduct a large set of simulations with different parameters and then find the SFD that resembles the observed one as accurately as possible. This makes the problem difficult as the parameter space is quite extensive. For one run, we usually have to specify the parent body size D_{pb}, the projectile size d_{project}, the impact speed v_{imp}, and the impact angle ϕ_{imp} (i.e. the angle between the velocity vector of the impactor and the inward normal of the target at the point of collision). Other parameters of the problem are the material properties of considered asteroids, such as bulk density, shear modulus, porosity etc.

Due to the extent of the parameter space, a thorough study would be highly demanding on computational resources. It is therefore reasonable to fix the size of the parent body and study breakups with various parameters of the impactor.

A large set of simulations was published by Durda et al. (2007), who studied disruptions of 100 km monolithic targets. Similarly, Benavidez et al. (2012) performed an analogous set of simulations with rubble-pile targets. They also used the resulting SFDs to estimate the size of the parent body for a number of asteroid families. As the diameter of the parent body is never exactly 100 km, the computed SFDs have to be multiplied by a suitable scaling factor f_{scale} to match the observed one. However, small families have been already discovered (e.g. Datura, Nesvorný et al. (2015)) and their parent-body size is likely $D_{\mathrm{pb}} = 10\,\mathrm{km}$, i.e. an order-of-magnitude smaller. The linearity of the scaling is a crucial assumption and we will assess the plausibility of this assumption in this paper.

To fill up a gap in the parameter space, we proceed with small targets. We carried out a set of simulations with $D_{\mathrm{pb}} = 10\,\mathrm{km}$ parent bodies and carefully compared them with the simulations of Durda et al. (2007).

The paper is organised as follows. In Section 2, we briefly describe our numerical methods. The results of simulations are presented in Section 3. Using the computed SFDs we derive parametric relations for the slope q and the masses M_{lr} and M_{lf} of the largest remnant and the largest fragment, respectively, in Section 4. Finally, we summarize our work in Section 5.

2. Numerical methods

We follow a hybrid approach of Michel et al. (2001, 2002, 2003, 2004), employing an SPH discretization for the simulation of fragmentation and an N-body integrator for subsequent gravitational reaccumulation. Each simulation can be thus divided into three phases: i) a fragmentation, ii) a hand-off, and iii) a reaccumulation. We shall describe them sequentially in the following subsections.

2.1. Fragmentation phase

The first phase of the collision is described by hydrodynamical equations in a lagrangian frame. They properly account for supersonic shock wave propagation and fragmentation of the material. We use the SPH5 code by Benz and Asphaug (1994) for their numerical solution. In the following, we present only a brief description of equations used in our simulations and we refer readers to extensive reviews of the method (Rosswog, 2009; Cossins, 2010; Price, 2008, 2012) for a more detailed description.

Our problem is specified by four basic equations, namely the equation of continuity, equation of motion, energy equation and Hooke's law:

$$\frac{\mathrm{d}\rho}{\mathrm{d}t} = -\rho\nabla\cdot\boldsymbol{v}\,, \tag{1}$$

$$\frac{\mathrm{d}\boldsymbol{v}}{\mathrm{d}t} = \frac{1}{\rho}\nabla\cdot\boldsymbol{\sigma}\,, \tag{2}$$

$$\frac{\mathrm{d}U}{\mathrm{d}t} = -\frac{P}{\rho}\mathrm{Tr}\,\dot{\boldsymbol{\epsilon}} + \frac{1}{\rho}\boldsymbol{S}:\dot{\boldsymbol{\epsilon}}\,, \tag{3}$$

$$\frac{\mathrm{d}\boldsymbol{S}}{\mathrm{d}t} = 2\mu\left(\dot{\boldsymbol{\epsilon}} - \tfrac{1}{3}\mathbf{1}\,\mathrm{Tr}\,\dot{\boldsymbol{\epsilon}}\right), \tag{4}$$

supplemented by the Tillotson equation of state (Tillotson, 1962). The notation is as follows: ρ is the density, $\boldsymbol{v}$ the speed, $\boldsymbol{\sigma}$ the stress tensor (total), where $\boldsymbol{\sigma} \equiv -P\mathbf{1} + \boldsymbol{S}$, P the pressure, $\mathbf{1}$ the unit tensor, $\boldsymbol{S}$ the deviatoric stress tensor, U the specific internal energy, $\dot{\boldsymbol{\epsilon}}$ the strain rate tensor, where $\dot{\boldsymbol{\epsilon}} \equiv \frac{1}{2}\left[\nabla\boldsymbol{v} + (\nabla\boldsymbol{v})^{\mathrm{T}}\right]$, with its trace $\mathrm{Tr}\,\dot{\boldsymbol{\epsilon}} = \nabla\cdot\boldsymbol{v}$, μ the shear modulus.

The model includes both elastic and plastic deformation, namely the yielding criterion of von Mises (1913) — given by the factor $f \equiv \min[Y_0^2/(\frac{3}{2}\boldsymbol{S}:\boldsymbol{S}), 1]$, **where Y_0 is the material depended yield stress** — and also failure of the material. The initial distribution of cracks and their growth to fractures is described by models of Weibull (1939) and Grady and Kipp (1980), which use a scalar parameter $\mathcal{D} \in \langle 0, 1\rangle$ called damage, as explained in Benz and Asphaug (1994). The stress tensor of damaged material is then modified as $\boldsymbol{\sigma} = -(1-\mathcal{D}H(-P))P\mathbf{1} + (1-\mathcal{D})f\boldsymbol{S}$, where $H(x)$ denotes the Heaviside step function. In this phase, we neglect the influence of gravity, which is a major simplification of the problem.

In a smoothed-particle hydrodynamic (SPH) formalism, Eqs. (1) to (4) are rewritten so as to describe an evolution of individual SPH particles (denoted by the index $i = 1..N$):

$$\frac{\mathrm{d}\rho_i}{\mathrm{d}t} = -\rho_i\sum_j \frac{m_j}{\rho_j}(\boldsymbol{v}_j - \boldsymbol{v}_i)\cdot\nabla W_{ij}\,, \tag{5}$$

$$\frac{\mathrm{d}\boldsymbol{v}_i}{\mathrm{d}t} = \sum_j m_j\left(\frac{\boldsymbol{\sigma}_i + \boldsymbol{\sigma}_j}{\rho_i\rho_j} + \Pi_{ij}\mathbf{1}\right)\cdot\nabla W_{ij}\,, \tag{6}$$

$$\frac{\mathrm{d}U_i}{\mathrm{d}t} = -\frac{P_i}{\rho_i}\sum_\gamma \dot{\epsilon}_i^{\gamma\gamma} + \frac{1}{\rho_i}\sum_\alpha\sum_\beta S_i^{\alpha\beta}\dot{\epsilon}_i^{\alpha\beta} + \left(\frac{\mathrm{d}U_i}{\mathrm{d}t}\right)_\Pi\,, \tag{7}$$

$$\frac{\mathrm{d}\boldsymbol{S}_i}{\mathrm{d}t} = 2\mu\left(\dot{\boldsymbol{\epsilon}}_i - \tfrac{1}{3}\mathbf{1}\sum_\gamma \dot{\epsilon}_i^{\gamma\gamma}\right), \tag{8}$$

with:

$$\dot{\epsilon}_i^{\alpha\beta} = \frac{1}{2\rho_i}\sum_j m_j\left[(v_j^\alpha - v_i^\alpha)\frac{\partial W_{ij}}{\partial x^\beta} + (v_j^\beta - v_i^\beta)\frac{\partial W_{ij}}{\partial x^\alpha}\right], \tag{9}$$

where m_j denote the masses of the individual SPH particles, $W_{ij} \equiv W(|\boldsymbol{r}_i - \boldsymbol{r}_j|, h)$ the kernel function, h the symmetrized

smoothing length, $h = \frac{1}{2}(h_i + h_j)$. Both the equation of motion and the energy equation were also supplied with the standard artificial viscosity term Π_{ij} (Monaghan and Gingold, 1983):

$$\Pi_{ij} = \begin{cases} \frac{1}{\rho}\left(-\alpha_{\mathrm{AV}} c_{\mathrm{s}} \mu_{ij} + \beta_{\mathrm{AV}} \mu_{ij}^2\right) & (\boldsymbol{v}_i - \boldsymbol{v}_j)\cdot(\boldsymbol{r}_i - \boldsymbol{r}_j) \le 0\,, \\ 0 & \text{otherwise}\,, \end{cases} \tag{10}$$

where:

$$\mu_{ij} = \frac{h(\boldsymbol{v}_i - \boldsymbol{v}_j)\cdot(\boldsymbol{r}_i - \boldsymbol{r}_j)}{\|\boldsymbol{r}_i - \boldsymbol{r}_j\|^2 + \epsilon h^2}\,, \tag{11}$$

c_{s} is the sound speed and $\alpha_{\mathrm{AV}}, \beta_{AV}$ **are free parameters of the viscosity model, values of which were** $\alpha_{\mathrm{AV}} = 1.5$ **and** $\beta_{\mathrm{AV}} = 3$ **as in Benz and Asphaug (1994). The corresponding term in the energy equation is then:**

$$\left(\frac{\mathrm{d}U_i}{\mathrm{d}t}\right)_{\Pi} = \sum_j \frac{1}{2}\Pi_{ij}(\boldsymbol{v}_i - \boldsymbol{v}_j)\cdot\nabla W_{ij}\,. \tag{12}$$

We sum over all particles, but since the kernel has a compact support, the algorithm has an asymptotic complexity $O(NN_{\mathrm{neighbours}})$. The actual number of SPH particles we used **(including both the particles of the target and the impactor)** is $N \doteq 1.4 \times 10^5$, and the number of neighbours is usually $N_{\mathrm{neighbours}} \simeq 50$. There is also an evolution equation for the smoothing length h_i in order to adapt to varying distances between SPH particles.

2.2. *Hand-off procedure*

Although SPH is a versatile method suitable for simulating both the fragmentation and the gravitational reaccumulation, the time step of the method is bounded by the Courant criterion and the required number of time steps for complete reaccumulation is prohibitive. In order to proceed with inevitably simplified but efficient computations, we have to convert SPH particles to solid spheres, a procedure called hand-off. In this paper, we compute the corresponding radius R_i as:

$$R_i = \left(\frac{3m_i}{4\pi\rho_i}\right)^{\frac{1}{3}}\,. \tag{13}$$

The time t_{handoff} at which the hand-off takes place is determined by three conditions:

1. It has to be at least $2D_{\mathrm{pb}}/c_{\mathrm{s}} \simeq 1\,\mathrm{s}$ (c_{s} being the sound speed), i.e. until the shock wave and rarefaction wave propagate across the target;
2. Fractures (damage) in the target should not propagate anymore, even though in catastrophic disruptions the shock wave usually damages the whole target and material is then practically strengthless;
3. The pressure in the fragmented parent body should be zero so that the corresponding acceleration $-\frac{1}{\rho}\nabla P$ is zero, or at least negligible. According to our tests for $D_{\mathrm{pb}} = 10\,\mathrm{km}$ targets, such relaxation takes up to 10 s.

On the other hand, there is an upper limit for t_{handoff} given by the gravitational acceleration of the target, $g = GM_{\mathrm{pb}}/R_{\mathrm{pb}}^2$, **where** $G \doteq 6.674 \times 10^{-11}\,\mathrm{m^3\,kg^{-1}\,s^{-2}}$ **is the gravitational constant.** This acceleration has to be small compared to the escape speed $v_{\mathrm{esc}} = \sqrt{2GM_{\mathrm{pb}}/R_{\mathrm{pb}}}$, i.e. a typical ejection speed v_{ej} of fragments. The corresponding time span should thus be definitely shorter than $v_{\mathrm{esc}}/g \simeq 10^3$ s.

2.3. *Reaccumulation phase*

Finally, gravitational reaccumulation of now spherical fragments is computed with an N-body approach. We use the `pkdgrav` code as modified by Richardson et al. (2000) for this purpose. It accounts for mutual gravitational interactions between fragments:

$$\ddot{\boldsymbol{r}}_i = -\sum_{j\neq i} \frac{Gm_j}{r_{ij}^3}\boldsymbol{r}_{ij}\,, \tag{14}$$

An $O(N^2)$ problem is simplified significantly using a tree code algorithm, i.e. by clustering fragments to cells and evaluating gravitational moments up to hexadecapole order, provided they fit within the opening angle $\mathrm{d}\theta = 0.5\,\mathrm{rad}$. The time step was $\Delta t = 10^{-6}$ (in $G = 1$ units, or about 5 s in SI), and the time span $50,000\,\Delta t$, long enough that the reaccumulation is over, or negligible.

Regarding mutual collisions, we assumed perfect sticking only, meaning no bouncing or friction. Consequently, we have no information about resulting shapes of fragments, we rather focus on their sizes, velocities and corresponding statistics.

3. A grid of simulations for $D_{\mathrm{pb}} = 10\,\mathrm{km}$ targets

We performed a number of simulations with $D_{\mathrm{pb}} = 10\,\mathrm{km}$ parent bodies, impact speed v_{imp} varying from 3 to 7 km/s, diameter d_{project} of the impactor from 0.293 km to 1.848 km (with a logarithmic stepping) and the impact angle ϕ_{imp} from 15° to 75°. The kinetic energy of the impact:

$$Q = \frac{\frac{1}{2}m_{\mathrm{project}}v_{\mathrm{imp}}^2}{M_{\mathrm{pb}}} \tag{15}$$

therefore varies from $\sim 10^{-2}Q_{\mathrm{D}}^\star$ to $\sim 20Q_{\mathrm{D}}^\star$, where $Q_{\mathrm{D}}^\star$ is the critical energy for shattering and dispersing 50% of the parent body. **The critical energy** $Q_{\mathrm{D}}^\star$ **is also used to compare runs with different size of parent body (see Sec. 3.4) We adopted** $Q_{\mathrm{D}}^\star(D)$ **values from the scaling law of basaltic materials and impact velocities** $v_{\mathrm{imp}} = 5\,\mathrm{km}$**, as given by Benz and Asphaug (1999). We use the same value of** $Q_{\mathrm{D}}^\star$ **for all impact velocities and impact angles, for simplicity. Using this scaling law, the critical energy for** $D_{\mathrm{pb}} = 10\,\mathrm{km}$ **is** $Q_{\mathrm{D}}^\star \simeq 7.68 \times 10^7\,\mathrm{erg/g}$**. For comparison, the critical energy for** $D_{\mathrm{pb}} = 100\,\mathrm{km}$ **is** $Q_{\mathrm{D}}^\star(10\,\mathrm{km}) \simeq 7.68 \times 10^7\,\mathrm{erg/g}$**, while for** $D_{\mathrm{pb}} = 100\,\mathrm{km}$**, the critical energy is** $Q_{\mathrm{D}}^\star(100\,\mathrm{km}) = 1.74 \times 10^9\,\mathrm{erg/g}$**. Note that the selected values** $Q_{\mathrm{D}}^\star$ **do not influence simulations at all, we use them as a base unit to get a convenient, dimensionless values of impact energies.**

The total number of performed runs is 125. We assume a monolithic structure of both the target and the impactor, and the material properties were selected those of basalt (summarized in Table 1).

Material parameters	
density at zero pressure	$\rho = 2700\,\mathrm{kg/m^3}$
bulk modulus	$A = 2.67 \times 10^{10}\,\mathrm{Pa}$
non-linear Tillotson term	$B = 2.67 \times 10^{10}\,\mathrm{Pa}$
sublimation energy	$u_0 = 4.87 \times 10^{8}\,\mathrm{J/kg}$
energy of incipient vaporization	$u_{\mathrm{iv}} = 4.72 \times 10^{6}\,\mathrm{J/kg}$
energy of complete vaporization	$u_{\mathrm{cv}} = 1.82 \times 10^{7}\,\mathrm{J/kg}$
shear modulus	$\mu = 2.27 \times 10^{10}\,\mathrm{Pa}$
von Mises elasticity limit	$Y_0 = 3.50 \times 10^{9}\,\mathrm{Pa}$
Weibull coefficient	$k = 4.00 \times 10^{29}$
Weibull exponent	$m = 9$

SPH parameters	
number of particles in target	$N_{\mathrm{pb}} \simeq 1.4 \times 10^{5}$
number of particles in projectile	$N_{\mathrm{pb}} = 100$ to 630
Courant number	$C = 1$
linear term of artificial viscosity	$\alpha_{\mathrm{AV}} = 1.5$
quadratic term of artificial viscosity	$\beta_{\mathrm{AV}} = 3.0$
duration of fragmentation phase	$t_{\mathrm{handoff}} = 10\,\mathrm{s}$

Table 1: Constant parameters used in our SPH simulations. **We assumed the same material parameters as Durda et al. (2007), which allows for ~~undistorted~~ comparison of results.** a direct

3.1. Size-frequency distributions

For each run we constructed a cumulative size-frequency distributions $N(>D)$ of fragments and we plotted them in Fig. 1. At first sight, the SFDs are well-behaved. Both cratering and catastrophic events produce mostly power-law-like distributions. Some distributions, mainly those around $Q/Q^{\star}_{\mathrm{D}} \sim 1$, have an increasing slope at small sizes (at around $D \sim 0.3$ km), but since this is close to the resolution limit, it is possibly a numerical artifact.

For supercatastrophic impacts with $d_{\mathrm{project}} = 1.848$ km, the distributions differ from power laws substantially; the slope becomes much steeper at large sizes of fragments. These are the cases where the gap between the largest remnant and the largest fragment disappears (we therefore say the largest remnant does not exist).

The situation is quite different for impacts with an oblique impact angle, mainly for $\phi_{\mathrm{imp}} = 75°$. We notice that these impacts appear much less energetic compared to other impact angles, even though the ratio $Q/Q^{\star}_{\mathrm{D}}$ is the same. The cause of this apparent discrepancy is simply the geometry of the impact. At high impact angles, the impactor does not hit the target with all its cross-section and a part of it misses the target entirely (grazing impacts, see Leinhardt and Stewart, 2012). Therefore, a part of the kinetic energy is not deposited into the target and the impact appears less energetic, compared to head-on impacts.

3.2. Speed histograms

Similarly to the size-frequency distributions, we computed speed distributions of fragments. The results are shown in Fig. 2. As we are computing an absolute value of the velocity, the resulting histogram depends on a selected reference frame. We chose a barycentric system for all simulations; however, we excluded high-speed remainders of the projectile with velocities $v_{\mathrm{ej}} > v_{\mathrm{cut}} \equiv 1$ km/s. These outliers naturally appear mainly for oblique impact angles. Because of very large ejection velocities, such fragments cannot belong to observed families and if we had included them in the constructed velocity field of the synthetic family, it would artificially shift velocities of fragments to higher values.

The main feature of cratering events is the peak around the escape velocity v_{esc}. This peak is created by fragments ejected at the point of impact. With an increasing impact energy, the tail of the histogram extends as the fragments are ejected at higher velocities.

Interestingly, there is a second peak at around $Q/Q^{\star}_{\mathrm{D}} \sim 0.3$. This is because of ejection of fragments from the antipode of the target. If the shockwave is energetic enough, it causes an ejection of many fragments. The second peak is barely visible at oblique impact angles. especially

One should be careful when interpreting the speed histograms of cratering events. The ejected fragments are ~~mostly~~ poorly resolved as they are mergers of only few SPH particles. It is not clear whether the resolution limit does not affect the histograms or it introduces a systematic bias. For mid-energy and catastrophic events, the fragments close to the resolutions limit fit mainly in the tail of the histogram and are of lesser importance to the result. often *2

3.3. Isotropy vs anisotropy of the velocity field

Fig. 3 shows angular distributions of the velocity fields in the plane of the impact. The histograms are drawn as polar plots with a 5° binning. The angles on plots correspond to the points of impact for given impact angle ϕ_{imp}; for cratering events, all the ejecta are produced at the point of impact and the distribution of fragments is therefore nicely clustered around ϕ_{imp}.

Cratering impacts tend to produce velocity fields mainly in the direction of the impact angle. Catastrophic impacts, on the other hand, generally produce much more isotropic velocity fields. However, the isotropy is not perfect, even though we removed outliers as above. Even for the supercatastrophic impacts, the number of fragments in different directions can vary by a factor of 5. Further changes of the reference frame may improve the isotropy. Note that for observed families, it is also not clear where is the reference points, as the identification of family members (and interlopers) is ambiguous.

3.4. A comparison with scaled-down $D_{\mathrm{pb}} = 100$ km simulations

To compare $D_{\mathrm{pb}} = 10$ km runs with $D_{\mathrm{pb}} = 100$ km runs, we need to choose collisions in approximately the same regimes (compare cratering events with cratering events, etc.). The regime can be determined using the scaling law, more specifically using the ratio $Q/Q^{\star}_{\mathrm{D}}$ ~~as a compared quantity.~~ We thus compare the runs with approximately the same ratio $Q/Q^{\star}_{\mathrm{D}}$ and the same impact angle. This means ~~the~~ impactors for 10 km runs are much smaller than the ones for 100 km runs, ~~as for $D_{\mathrm{pb}} = 10$ km bodies~~, As we require the same $Q/Q^{\star}_{\mathrm{D}}$ ratio for ~~compared~~ simulations, in or ϕ_{imp} the two (even relatively)

*2 When we drop the smallest particles from the distribution, the overall velocities are slightly lower, but this is also an expected outcome due to ~~an~~ the equipartition theorem which approximately holds for these collisions. even

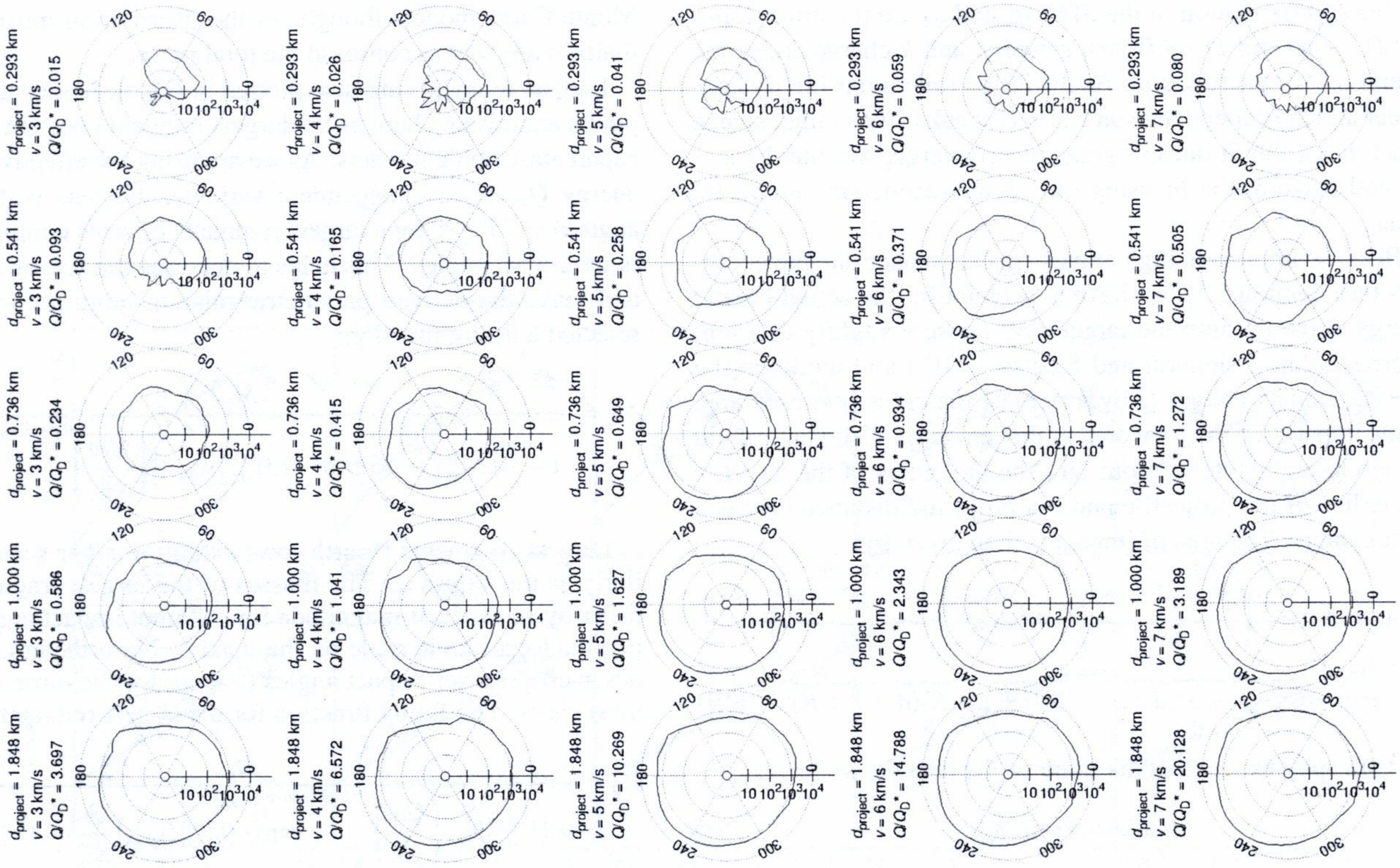

Figure 3: Histograms of velocity angular distribution (in the plane of the collision) of fragments. The velocities are evaluated in the barycentric coordinate system with outliers removed. The angle 180° corresponds to the velocity direction of the projectile. The impact angle $\phi_{\rm imp} = 45°$.

was a slightly

some cases it is necessary to select different impact velocities, as all 100km runs with the same velocity as the considered 10km have significantly different ratio $Q/Q_{\rm D}^\star$; for example the $D_{\rm pb} = 10\,{\rm km}$ simulation with $d_{\rm project} = 0.736\,{\rm km}$ and $v_{\rm imp} = 5\,{\rm km/s}$ is being compared to $D_{\rm pb} = 100\,{\rm km}$ simulation with $d_{\rm project} = 18\,{\rm km}$ and $v_{\rm imp} = 6\,{\rm km/s}$.

Looking at Fig. 1., we can see that the mid-energy events with $Q/Q_{\rm D}^\star \sim 1$ have SFDs comparable to scaled 100 km ones. In this regime, down-scaling of the distribution for $D_{\rm pb} = 100\,{\rm km}$ targets seems to be a justifiable way to approximate SFDs for targets of smaller sizes. **There is also a noticeable dependence on impact angle, probably due to different sizes of impactors in corresponding simulations. Comparing the SFDs with the best match for each impact angle, we can see that for $\phi_{\rm imp} = 15°$ this best match of SFDs is achieved in interval $Q/Q_{\rm D}^\star = 0.4$ to 0.9; for $\phi_{\rm imp} = 30°$ this matching interval is shifted to $Q/Q_{\rm D}^\star = 0.5$ to 1.0, and for $\phi_{\rm imp} = 45°$, the interval is further moved to $Q/Q_{\rm D}^\star = 1.0$ to 3.0. The match between both sets of SFDs is generally worse for impact angles 60° and 75° due to geometric effect mentioned in Sec. 3.1.**

In case of cratering events, our simulations differ significantly from scaled ones. Impacts into 10 km targets produce a much shallower fragment distribution compared to 100 km impacts; see impacts with $d_{\rm project} = 0.293\,{\rm km}$. We also note that supercatastrophic runs have different outcomes than the 100 km ones; our distributions are much shallower and have a much larger largest fragment. **Note that even though the 100km bodies have higher self-gravity and a bigger largest fragment compared to the 10km runs might be expected, the higher self-gravity is already accounted for in the critical energy $Q_{\rm D}^\star$.** The $D_{\rm pb} = 10\,{\rm km}$ supercatastrophic impacts also also produce a steeper part of the SFD at larger diameters, which is *not* visible for 100 km simulations, at least not to the same extent.

4. Parametric relations for Monte-Carlo collisional models

Size-frequency distributions constructed from our simulations consist mostly of three parts: the largest remnant separated from the fragments, the middle part of the SFD with a power-law shape (in log-log plot) and a "staircase" of small fragments, marking the resolution limit of our simulation. Ignoring the staircase, the slope of the middle part between $D = 0.3$ and 2 km can be fitted with a linear function:

$$\log N(>D) = q \log[D]_{\rm km} + c\,. \qquad (16)$$

Supercatastrophic events behave differently though, and their SFDs can be well fitted with a two-slope function:

$$\log N(>D) = K\,(\log[D]_{\rm km} - \log[D_0]_{\rm km}) + c\,, \qquad (17)$$

where:

$$K(x) = \frac{1}{2}(q_1 + q_2)x + \frac{1}{2}\frac{q_1 - q_2}{k}\log(2\cosh kx)\,. \qquad (18)$$

In this approximation of the SFD, q_1 and q_2 are the limit slopes for $D \to \infty$ and $D \to 0$, respectively, and k characterizes the "bend-off" of the function. As the fitting function is highly non-linear and the dependence on k is very weak (given rather sparse input data), the fit doesn't generally converge, we thus fix $k = 10$ and perform the fit using only four parameters: q_1, q_2, D_0 and c.

Because impacts at high angles appear weaker due the geometry (see Section 3.1), we have to account for the actual kinetic energy delivered into the target. We chose a slightly different approach than Leinhardt and Stewart (2012) and modified the specific impact energy Q by a ratio of the cross-sectional area of the impact and the total area of the impactor. Using a formula for circle-circle intersection: let R be the radius of the target, r the radius of the projectile and d a projected distance between their centers. The area of impact is then given by:

$$A = r^2 \cos^{-1}\left(\frac{d^2 + r^2 - R^2}{2dr}\right) + R^2 \cos^{-1}\left(\frac{d^2 + R^2 - r^2}{2dR}\right) - \\ - \frac{1}{2}\sqrt{(R + r - d)(d + r - R)(d - r + R)(d + r + R)}\,. \quad (19)$$

As both spheres touch at the point of the impact, we have:

$$d = (r + R)\sin\phi_{\mathrm{imp}}\,. \quad (20)$$

Using these auxiliary quantities, we define the *effective* specific impact energy:

$$Q_{\mathrm{eff}} = Q\frac{A}{\pi r^2}\,. \quad (21)$$

In Fig. 4, we separately plot slopes q, constants c of the linear fits of the SFDs, and the masses of the largest remnants M_{lr} and largest fragment M_{lf}. Each of these quantities shows a distinct dependence on the impact speed v_{imp}, suggesting parametric relations cannot be well described by a single parameter $Q_{\mathrm{eff}}/Q_{\mathrm{D}}$. We therefore plot each dependence separately for different v_{imp} and we explicitly express the dependence on v_{imp} in parametric relations.

For low speeds, slopes q can be reasonably fitted with a function:

$$q = -12.3 + 0.75 v_{\mathrm{imp}} + \frac{(11.5 - 1^{+0.2}_{-0.1} v_{\mathrm{imp}}) \exp\left(-5 \cdot 10^{-3} \dfrac{Q_{\mathrm{eff}}}{Q^\star_{\mathrm{D}}}\right)}{1 + 0.1^{+0.01}_{-0.02}\left(\dfrac{Q_{\mathrm{eff}}}{Q^\star_{\mathrm{D}}}\right)^{-0.4}}, \quad (22)$$

where v_{imp} is expressed in km/s. However, for high speeds (especially for $v = 7$ km/s), the individual values of q for different impact angles differ significantly and thus the fit has a very high uncertainty. We account for this behaviour in Eq. (22), where the uncertainty increases with an increasing speed.

The constant c can be well fitted by linear function:

$$c = 0.9 + 2.3\exp(-0.35 v_{\mathrm{imp}}) + \left(1.3 - 0.1 v_{\mathrm{imp}}\right)\left(\frac{Q_{\mathrm{eff}}}{Q^\star_{\mathrm{D}}}\right). \quad (23)$$

The high scatter noted in the parametric relation for the slope q is not present here. This parameter is of lesser importance for Monte-Carlo models though, as the distribution must be normalized anyway to conserve the total mass.

Largest remnants are also plotted in Fig. 4. Notice that some points are missing here as the largest remnant does not exist for supercatastrophic impacts. As we are using the effective impact energy Q_{eff} as an independent variable, the runs with impact angle $\phi = 75°$ produce largest remnants of sizes comparable to other impact angles. This helps to decrease the scatter of points and make the derived parametric relation more accurate. We selected a fitting function:

$$M_{\mathrm{lr}} = \frac{M_{\mathrm{tot}}}{1 + \left[0.6^{+0.5}_{-0.2} + 56\exp(-1.0^{+0.6}_{-0.2} v_{\mathrm{imp}})\right]\left(\dfrac{Q_{\mathrm{eff}}}{Q^\star_{\mathrm{D}}}\right)^{0.8+8\exp(-0.7 v_{\mathrm{imp}})}}. \quad (24)$$

Largest fragments (fourth row) exhibit a larger scatter, similarly as the slopes q. The masses of the largest fragment can differ by an order of magnitude for different impact angles (notice the logarithmic scale on the y-axis). Nevertheless, the values averaged over impact angles (red circles) lie close the fit in most cases. The fitting function for the largest remnant is:

$$M_{\mathrm{lf}} = \frac{M_{\mathrm{tot}}}{0.24^{+0.60}_{-0.15} v^3_{\mathrm{imp}}\left(\dfrac{Q_{\mathrm{eff}}}{Q^\star_{\mathrm{D}}}\right)^{-0.6-2\exp(-0.3 v_{\mathrm{imp}})} + \exp\left(-0.3^{+0.2}_{-0.2} v_{\mathrm{imp}}\right)\dfrac{Q_{\mathrm{eff}}}{Q^\star_{\mathrm{D}}} + 11^{+15}_{-8} + 2 v_{\mathrm{imp}}}. \quad (25)$$

This function bends and starts to decrease for $Q_{\mathrm{eff}}/Q^\star_{\mathrm{D}} \gg 1$. Even though this behaviour is not immediately evident from the plotted points, the largest fragment *must* become a decreasing function of impact energy in the supercatastrophic regime.

The derived relations could be compared with relations for $D_{\mathrm{pb}} = 100$ km bodies, published in Cibulková et al. (2014). The comparison is not straightforward, ~~however~~, as we chose different fitting functions and also different variables to parametrize the relations. Nevertheless, the parametric relations only approximate SFDs ~~and~~ the differences between SFDs of $D_{\mathrm{pb}} = 10$ km and 100 km bodies have already been discussed in Sec. 3.4.

5. Conclusions and future work

In this paper, we studied disruptions and subsequent gravitational reaccumulation of asteroids with diameter $D_{\mathrm{pb}} = 10$ km. Using an SPH code and an efficient N-body integrator, we performed impact simulations for various projectile sizes d_{project}, impact speeds v_{imp} and angles ϕ_{imp}. The size-frequency distributions, constructed from the results of our simulations, appear similar to the scaled-down simulations of Durda et al. (2007) only in the transition regime between cratering and catastrophic events ($Q/Q^\star_{\mathrm{D}} \simeq 1$); however, they differ significantly for both the weak cratering impacts and for supercatastrophic impacts.

The resulting size-frequency distributions can be used to estimate the size of the parent body, especially for small families. As an example, we used our set of simulations to determine D_{pb} of the Karin family. This cluster was studied in detail by Nesvorný et al. (2006) and we thus do not intend to increase the accuracy of their result, but rather to assess the uncertainty

of linear SFD scaling. The closest fit to the observed SFD of the Karin cluster yields a parent body with $D_{\rm pb} = 25\,$km — a smaller, but comparable value to $D_{\rm pb} = 33\,$km, obtained by Nesvorný et al. (2006). Using the set of $D_{\rm pb} = 100\,$km simulations, Durda et al. (2007) obtained an estimate $D_{\rm pb} \simeq 60\,$km. It is therefore reasonable that the best estimate is intermediate between the result from upscaled 10 km runs and downscaled 100 km runs. We do not consider our result based on "generic" simulations more accurate than the result of Nesvorný et al. (2006); however, the difference between the results can be seen as an estimate of uncertainty one can expect when scaling the SFDs by a factor of 3.

We derived new parametric relations, describing the masses $M_{\rm lr}$ and $M_{\rm lf}$ of the largest remnant and the largest fragment, respectively, and the slope q of the size-frequency distribution as functions of the impact parameters. These parametric relations can be used straightforwardly to improve the accuracy of collisional models, as the fragments created by a disruption of small bodies were previously estimated as scaled-down disruptions of $D_{\rm pb} = 100\,$km bodies.

In our simulations, we always assumed monolithic targets. The results can be substantially different for porous bodies, though, as the internal friction has a significant influence on the fragmentation (Jutzi et al., 2015; Asphaug et al., 2015). This requires using a different yielding model, such as Drucker–Prager criterion. We postpone a detailed comparison between monolithic and porous bodies for future work.

Acknowledgements

The work of MB and PŠ was supported by the Grant Agency of the Czech Republic (grant no. P209/15/04816S).

Appendix A. Initial distribution of SPH particles

For a unique solution of evolutionary differential equations, initial conditions have to be specified. In our case, this means setting the initial positions and velocities of SPH particles. We assume non-rotating bodies, all particles of the target are therefore at rest and all particles of the impactor move with the speed of the impactor.

Optimal initial positions of SPH particles have to meet several criteria. First of all, the particles have to be distributed evenly in space. This requirement eliminates a random distribution as a suitable method, for using such a distribution would necessarily lead to clusters of particles in some parts of space and a lack of particles in other parts.

We therefore use a hexagonal-close-packing lattice in the simulations. They are easily set up and have an optimal interpolation accuracy. However, no lattice is *isotropic*, so there are always preferred directions in the distribution of SPH particles. This could potentially lead to numerical artifacts, such as pairing instability (Herant, 1994). Also, since the particle concentration is uniform, the impact is therefore resolved by only a few SPH particles for small impactors. We can increase accuracy of cratering impacts by distributing SPH particles nonuniformly, putting more particles at the point of impact and fewer in more distant places.

Here we assess the uncertainty introduced by using different initial conditions of SPH particles. A suitable method for generating a nonuniform isotropic distribution has been described by Diehl et al. (2012) and Rosswog (2015). Using initial conditions generated by this method, we ran several SPH/N-body simulations, and we compared the results to the simulations with lattice initial conditions.

The comparison is in Fig. A.5. Generally, the target shatters more for the nonuniform distribution. The largest remnant is smaller; the difference is up to 10% for the performed simulations. There are also more fragments at larger diameters, compared to the lattice distribution. This is probably due to slightly worse interpolation properties of the nonuniform distribution. A test run for a *random* distribution of particles led to a complete disintegration of the target and a largest remnant smaller by an order of magnitude, suggesting the smaller largest remnant is a numerical artifact of the method. On the other hand, the SFD is comparable at smaller diameters. This leads to more bent, less power-law-like SFDs for nonuniform runs.

Appendix B. Sensitivity to Weibull parameters

In the computed grid of simulations, we kept all the material parameters fixed to the nominal values listed in Table 1. We did not study the dependence of the resulting distributions $N(>D)$ and $\mathrm{d}N(v)/\mathrm{d}v$ on these parameters, as the size of the parameter space would be exceedingly large, and also to make the comparison with 100km runs of Durda et al. (2007) easier; both sets of simulation used the same material parameters.

However, the fragmentation process is mainly determined by the flaw distribution in the selected material, approximated by the Weibull power-law (Weibull, 1939):

$$n(\epsilon) = k\epsilon^m\,, \tag{B.1}$$

where m is the Weibull exponent and k is the normalization coefficient. For basaltic material, the Weibull exponent can range from $m = 6$ to 12 (Jaeger et al., 2007) and the coefficient k can possibly vary by an order of magnitude, making them the most uncertain material parameters.

To assess the uncertainty which propagates to the resulting SFDs, we ran a few simulations with $d_{\rm project} = 0.736\,$km, $v_{\rm imp} = 5\,$km and $\phi_{\rm imp} = 45°$, varying the Weibull parameters. Two simulations have different ~~Weibull~~ exponent, $m = 6$ and $m = 12$, two simulations differ in the coefficient k. The produced SFDs can be seen in Fig. B.6. As expected, the differences between individual runs are noticeable, however, they do not change the overall characteristics of SFD. The slope of the SFD between $D = 0.3$ and 1 km is approximately the same (within 0.2) in all runs, while the sizes of the largest remnant differ in a predictable way: more flaws with higher activation strain means higher fragmentation and subsequently smaller largest remnant. We can conclude that the Weibull parameters may introduce a

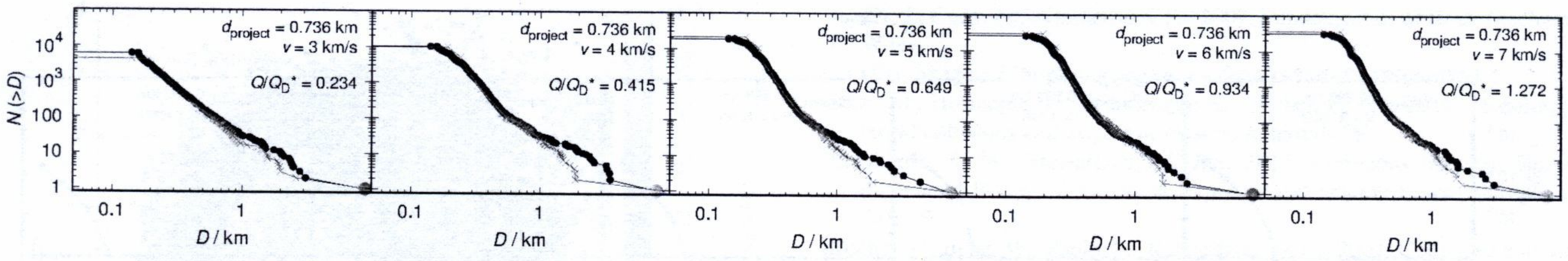

Figure A.5: SFDs constructed from five different simulations with $D_{\text{pb}} = 10\,\text{km}$, $d_{\text{project}} = 0.736\,\text{km}$ and impact angle $\phi_{\text{imp}} = 45°$. Black histogram shows the runs with the nonuniform distribution generated by the method of Diehl et al. (2012), while red are the previous (lattice) results shown in Fig. E.11.

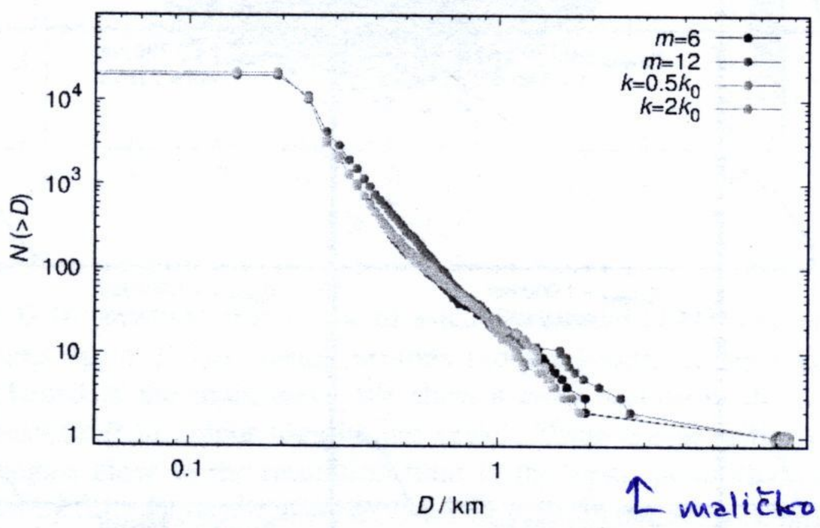

Figure B.6: Size-frequency distributions for various Weibull parameters k and m. Here $k_0 = 4.0 \times 10^{29}$ is the nominal value used in main text, see Table 1.

(systematic) uncertainty, but there are also other model parameters, for example the initial distribution of SPH particles, which may result in a bias of similar order.

Appendix C. Energy conservation vs. timestepping

Modelling of smaller breakups seems more difficult. Apart from poor resolution of the impactor, if one uses the same (optimum) SPH particle mass as in the target, and a relatively low number of ejected fragments, weak impacts may also exhibit problems with energy conservation (see Fig. C.7). This is even more pronounced in the case of low-speed collisions, e.g. of $D = 1\,\text{km}$ target, $d = 22\,\text{m}$ projectile, at $v_{\text{imp}} = 3\,\text{km/s}$ and $\phi_{\text{imp}} = 45°$.

At first, we thought that small oscillations of density — with relative changes $\Delta\rho/\rho$ smaller than the numerical precision — are poorly resolved, and subsequently cause the total energy to increase. But when we performed the same simulation in quadruple precision (with approximately 32 valid digits) we realised there is essentially no improvement (see Fig. C.8), so this cannot be the true reason.

Instead, we changed the timestepping scheme and superseded the default predictor/corrector with the Bulirsch–Stoer integrator (Press et al., 1992), which performs a series of trial steps with Δt divided by factors $2, 4, 6, \ldots$, and checks if the relative difference between successive divisions is less than small dimensionless factor ϵ_{BS} and then extrapolates to $\Delta t \to 0$. In our case, a scaling of quantities is crucial. In principle, we have three options: (i) scaling by expected maximum values, which results in a constant absolute error; (ii) current values, or constant relative error; (iii) derivatives times time step, a.k.a. constant cumulative error. The option (i) seems the only viable one, otherwise the integrator is exceedingly slow during the initial pressure build-up. According to Fig. C.9, we have managed to somewhat improve the energy conservation this way, but more work is needed to resolve this issue.

Appendix D. Energy conservation vs sub-resolution acoustic waves

Even though we always start with intact monolithic targets, we realized that prolonged computations of the fragmentation phase require a more careful treatment of undamaged/damaged boundaries. The reason is the following rather complicated mechanism: (i) The shock wave, followed by a decompression wave, *partially* destroys the target. After the reflection from the free surface, the rarefaction (or sound) wave propagates back to the target. (ii) However, neither wave can propagate into already damaged parts, so there is only an undamaged cavity. (iii) This cavity has an *irregular* boundary, so that reflections from it create a lot of small waves, interfering with each other. (iv) As a result of this interference, there is a lot of particles that have either high positive or high negative pressure, so that the pressure gradient — computed as a sum over neighbours — is *zero*! (v) $\nabla P = 0$ means no motion, and consequently no pressure release is possible. (vi) However, at the *boundary* between undamaged/damaged material, there are some particles with $P > 0$, next to the damaged ones with $P = 0$, which slowly push away the undamaged particles in the surroundings. (vii) Because the pressure is still not released, the steady pushing eventually destroys the whole target (see Fig. D.10).

In reality, this does not happen, because the waves can indeed become very small and dissipate. In SPH, the dissipation of waves at the resolution limit is impossible. Increasing resolution does not help at all — the boundary is even more irregular and the sound waves will anyway become as small as the resolution.

As a solution, we can use an upper limit for damage, very close to 1, but not equal to 1, e.g. $(1 - \mathcal{D}) = 10^{-12}$. Then the acoustic waves are damped (in a few seconds for $D = 1\,\text{km}$ targets) and the energy is conserved perfectly. Another option would be to use a more detailed rheology of the material, namely the internal friction and Drucker–Prager yield criterion (as in Jutzi et al., 2015).

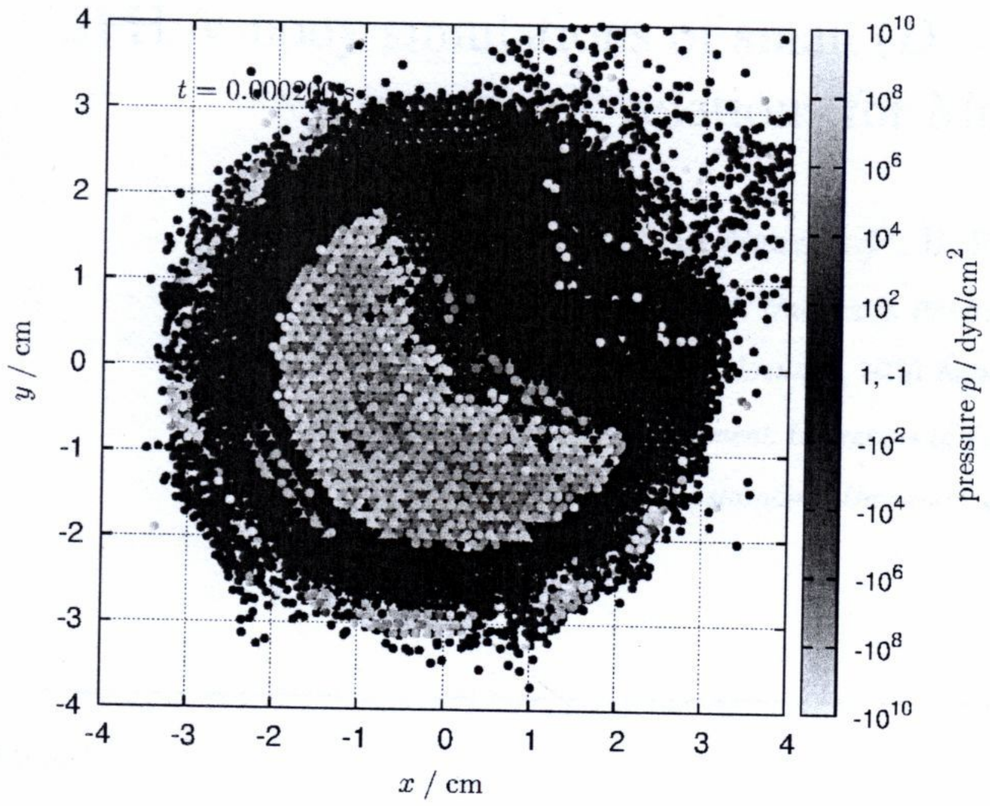

Figure D.10: A simulation of the classical Nakamura (1993) experiment, but prolonged up to 200 μs, which exhibits problems with energy conservation, as explained in the main text. We show a cross section in the (x, y) plane and pressure P in colour logarithmic scale. There are acoustic waves with wavelengths close to the resolution limit in the inner monolithic cavity, surrounded by fully damaged material (with $\mathcal{D} = 1$). In our setup, $D_{\text{target}} = 6\,\text{cm}$, $d_{\text{project}} = 0.7\,\text{cm}$, $\rho = 2.7$, or $1.15\,\text{g cm}^{-3}$ respectively, $v_{\text{imp}} = 3.2\,\text{km s}^{-1}$, $\phi_{\text{imp}} = 30°$, $N_{\text{part}} \doteq 7 \cdot 10^5$.

Appendix E. Additional figures

Figures D. 10 to D. 21 show the situation for non-standard impact angles.

Asphaug, E., Collins, G., Jutzi, M., 2015. Global scale impacts. Asteroids IV, 661–677.

Benavidez, P. G., Durda, D. D., Enke, B. L., Bottke, W. F., Nesvorný, D., Richardson, D. C., Asphaug, E., Merline, W. J., May 2012. A comparison between rubble-pile and monolithic targets in impact simulations: Application to asteroid satellites and family size distributions. Icarus 219, 57–76.

Benz, W., Asphaug, E., Jan. 1994. Impact simulations with fracture. I - Method and tests. Icarus 107, 98.

Benz, W., Asphaug, E., Nov. 1999. Catastrophic Disruptions Revisited. Icarus 142, 5–20.

Cibulková, H., Brož, M., Benavidez, P. G., Oct. 2014. A six-part collisional model of the main asteroid belt. Icarus 241, 358–372.

Cossins, P. J., Jul. 2010. The Gravitational Instability and its Role in the Evolution of Protostellar and Protoplanetary Discs. Ph.D. thesis, University of Leicester.

Davis, D. R., Ryan, E. V., 1990. On collisional disruption: Experimental results and scaling laws. Icarus 83 (1), 156–182.

Diehl, S., Rockefeller, G., Fryer, C. L., Riethmiller, D., Statler, T. S., Nov. 2012. Generating Optimal Initial Conditions for Smooth Particle Hydrodynamics Simulations. ArXiv e-prints.

Durda, D. D., Bottke, W. F., Nesvorný, D., Enke, B. L., Merline, W. J., Asphaug, E., Richardson, D. C., Feb. 2007. Size-frequency distributions of fragments from SPH/N-body simulations of asteroid impacts: Comparison with observed asteroid families. Icarus 186, 498–516.

Grady, D., Kipp, M., 1980. Continuum modelling of explosive fracture in oil shale. International Journal of Rock Mechanics and Mining Sciences & Geomechanics Abstracts 17 (3), 147 – 157.

Herant, M., 1994. Dirty Tricks for SPH (Invited paper) 65, 1013.

Herrmann, W., 1969. Constitutive equation for the dynamic compaction of ductile porous materials. Journal of Applied Physics 40 (6), 2490–2499.

Hirayama, K., Oct. 1918. Groups of asteroids probably of common origin. AJ31, 185–188.

Jaeger, J., Cook, N., Zimmerman, R., 2007. Fundamentals of Rock Mechanics. Wiley.
URL https://books.google.cz/books?id=FqADDkunVNAC

Jutzi, M., Holsapple, K., Wünneman, K., Michel, P., Feb. 2015. Modeling asteroid collisions and impact processes. Asteroids IV.

Leinhardt, Z. M., Stewart, S. T., Jan. 2012. Collisions between Gravity-dominated Bodies. I. Outcome Regimes and Scaling Laws. Astrophys. J. 745, 79.

Michel, P., Benz, W., Paolo, T., Richardson, D. C., 2001. Collisions and gravitational reaccumulation: Forming asteroid families and satellites. Science 294 (5547), 1696–1700.

Michel, P., Benz, W., Richardson, D. C., Feb. 2003. Disruption of fragmented parent bodies as the origin of asteroid families. Nature 421, 608–611.

Michel, P., Benz, W., Richardson, D. C., Apr. 2004. Catastrophic disruption of pre-shattered parent bodies. Icarus 168, 420–432.

Michel, P., Jutzi, M., Richardson, D. C., Benz, W., Jan. 2011. The Asteroid Veritas: An intruder in a family named after it? Icarus 211, 535–545.

Michel, P., Tanga, P., Benz, W., Richardson, D. C., 2002. Formation of asteroid families by catastrophic disruption: Simulations with fragmentation and gravitational reaccumulation. Icarus 160 (1), 10 – 23.

Monaghan, J., Gingold, R., 1983. Shock simulation by the particle method sph. Journal of Computational Physics 52 (2), 374 – 389.

Morbidelli, A., Bottke, W. F., Nesvorný, D., Levison, H. F., Dec. 2009. Asteroids were born big. Icarus 204, 558–573.

Nakamura, A., Fujiwara, A., Jul. 1991. Velocity distribution of fragments formed in a simulated collisional disruption. Icarus 92, 132–146.

Nesvorný, D., Brož, M., Carruba, V., Feb. 2015. Identification and Dynamical Properties of Asteroid Families. Asteroids IV.

Nesvorný, D., Enke, B. L., Bottke, W. F., Durda, D. D., Asphaug, E., Richardson, D. C., Aug. 2006. Karin cluster formation by asteroid impact. Icarus 183, 296–311.

Press, W. H., Teukolsky, S. A., Vetterling, W. T., Flannery, B. P., 1992. Numerical recipes in FORTRAN. The art of scientific computing.

Price, D. J., Dec. 2008. Modelling discontinuities and Kelvin Helmholtz instabilities in SPH. Journal of Computational Physics 227, 10040–10057.

Price, D. J., Feb. 2012. Smoothed particle hydrodynamics and magnetohydrodynamics. Journal of Computational Physics 231, 759–794.

Richardson, D. C., Quinn, T., Stadel, J., Lake, G., Jan. 2000. Direct Large-Scale N-Body Simulations of Planetesimal Dynamics. Icarus 143, 45–59.

Rosswog, S., Apr. 2009. Astrophysical smooth particle hydrodynamics. New A Rev.53, 78–104.

Rosswog, S., Apr. 2015. Boosting the accuracy of SPH techniques: Newtonian and special-relativistic tests. Mon. Not. R. Astron. Soc. 448, 3628–3664.

Tillotson, J. H., Jul. 1962. Metallic equations of state for hypervelocity impact. General Atomic Report GA-3216.

von Mises, R., 1913. Mechanik der festen krper im plastisch- deformablen zustand. Nachrichten von der Gesellschaft der Wissenschaften zu Gttingen, Mathematisch-Physikalische Klasse 1913, 582–592.

Weibull, W., 1939. A Statistical Theory of the Strength of Materials. Ingeniörsvetenskapsakademiens handlingar. Generalstabens litografiska anstalts förlag.

sjednotit mezerování

Reviewer 1

> Please find enclosed my review of the paper " SPH/N-body simulations of
> small (D=10 km) asteroidal breakups and improved parametric relations for
> MonteCarlo collisional models" by Broz et al., submitted to Icarus. In this
> work, the authors present a new set of impact simulation, extending the
> Durda et al. (2007) study to D=10 km. In addition, they use this new set of
> simulation to derive parametric relations, which could be useful as input in
> collisional models, in particular to study asteroid families formations.

> Overall I feel that this work is a good attempt to merge new data in order
> to constrain the physical properties of asteroids. I recommend the submitted
> paper for publication with moderate revision.

> I have a list of points that deserve some comments and/or changes, which are
> not listed in strict order of importance.

> Section 2.1

> - Line 117, Y_0 is not defined.

> - Equations 7 to 9, \alpha, \beta and \gamma superscript are not defined.

> - Also at line 133 the authors give values for \alpha_AV and \beta_AV, which
> do not appear in any equation. I guess these refer to alpha and beta in
> equation 10, but subscripts are missed and that fact could confuse the
> reader. So, this paragraph would be more readable if every constant is
> explicitly defined.

We would like to thank the referee for carefully reading the text and pointing out the missing definitions. Each quantity is now properly defined in the resubmitted manuscript.

> - Line 135, Is N the same that N_pb + N_p in table 1? The number does not
> agree. Beside, check in table 1 N_pb is used for the number of particles in
> the target and for the projectile also.

Here, we mainly wanted to give an order-of-magnitude comparison between the total number of particles (N) and number of neighbours (N_neighbours). However, it could be confusing for the reader that the number is different than the one used in Table 1. To be consistent, we changed N to 1.4 x 10^5 in the text.

> - Line 156, define G (the gravity constant) please.

The gravitational constant G is now defined in the text.

> Section 3.1
> - This comment applies to all of the size distribution plots (Fig.1 and D.10.
> to D.13). A significant fraction of the plot is used up by the "stair case"
> from 1000 to 10^4 (and y-axis extend up to 10^5), this is due to the
> resolution limit and not an interesting bit to be plotting. I recommend stop
> at halfway between 1000 and 10^4 and give more space to the resolved section
> of the size distribution.

We beg to disagree on this point. Referee is absolutely right that the "staircase" part of the plot is not relevant result from the physical point of view, on the other hand it clearly shows the resolution limit and sizes of the smallest fragments in the simulation. We believe it is an important feature of the plots for numerical reasons and we would rather leave the plots unchanged.

Nevertheless, we added a „warning" for readers...

In electronic form, the plots can be zoomed-in.

> - Line 177: Given Benz and Asphaug (1999) derived the scaling law from impact
> simulations at impact speed of 3 and 5 km/s. It is worst to give some more

> details about the procedure to estimate Q^*_D for every impact conditions of
> the present article. It is said, did you make any estimation to get Q^*_D for
> each impact speed and projectile size? Could you provide the value assumed
> for Q^*_D?

> - Related to this, in caption of figure 1: the authors said -To compare
> Åapples with apples, we compare runs with (approximately) the same Q/Q^*_D
> ratios and the same impact angle¸. Given that all the comparison is base on
> this equivalence, it could be useful for the reader to have some example or
> illustrate in some way the correspondence (in terms of impact parameters)
> between D=10 km and D=100 km runs with the same Q/Q^*_D ratio.

corresponding to the scaling law derived by Benz & Asphaug for D = 10 km and for the ...

We agree with the referee, the scaling law and Q^*_D values are not explained sufficiently. To explain, we used ~~the same~~ values of Q^*_D ~~for all performed simulations, using the scaling law derived for~~ impact velocity v_imp=5 km/s. This makes it easier to compare different runs. We expanded this section in the resubmitted manuscript, adding above mentioned and also the exact values of Q^*_D for 10km and 100km bodies. Furthermore, we give an example of how the corresponding D_pb=100km simulations were selected, see Sec. 3.4.

> Section 3.2.
> -At previous section (3.1) you mention that the resolutions limit is around D
> =0.3 km. In this section it could be included some comments about if you had
> removed these fragments from the histogram or if you have checked if these
> smaller fragments produce any bias on the speed distribution.

This is an interesting point that we did not address in the paper. Small fragments close to the resolution limit are of little importance for histograms of supercatastrophic impacts, but they are certainly significant for cratering impacts, as the families created by cratering events consist of only few particles and the majority of particles form the largest remnant. We added a note about the issue in Sec. 3.2 of the revised manuscript.

> Section 3.4
> - This section attempt to address the global SFD comparison for impacts into
> D=10 km target and the scaled-down D=100 km from Durda et al. (2007).
> Reading this section one can think that always Q/ Q^*_D ~~ 1convenite t could
> be convenitnetever, analising every figure for diffeent if these samller
> fragments be include some comments convenite t could be convenitnetever,
> analising every figure for diffeent if these samller fragments be include
> some comments , it is suitable to scale the SFDs. However, analysing every
> figure for different impact angles including D.10 to D.13 I see that this
> condition does not apply for all impact angles. For instance, at impact
> angles of 15 and 30 the comparable SFDs seem to be those with Q/Q^*_D
> around 0.6 and 0.9. However at 45 such range shifts to 1.2 to about 3, and
> for more oblique impact angle it is no possible to match the SFD.

wtf ? :-1

> In order to be more consistent with what figures show, I consider that it
> might be convenient to soften this claim and include a more detailed
> discussion for different angles.

We thank the referee for pointing out the dependence of SFDs on impact angle that we did not mention in the paper. We believe it does not invalidate our claims, though. For all impact angles, the best correspondence between the 10km and 100km runs is achieved in the mid-energy regime and the differences are larger in both the cratering and the catastrophic regime. However, the best match clearly depends on impact angle as mentioned by the referee, ~~probably~~ because of different projectile sizes in both compared simulations. We discuss this dependence in more detail in Sec. 3.4 of the paper.

> - At the end of this section, the authors explain the different SFD behaviour
> for supercatastrophic impacts. It would be expected that larger targets
> produce larger largest remnant due to self-gravity. Could the authors offer
> any discussion for this outcome?

Regarding this point, we argue that the higher self-gravity of the 100km bodies is already accounted for in the critical energy Q^*_D; the energy is considerably higher compared to D_pb=10km bodies. Impact to D=100km body with given ratio Q/Q_D^* does not necessarily produce a bigger largest remnant (fragment) compared to impact to D=10km body with the same Q/Q_D^*, actually the largest fragment seems to be smaller for D=100km bodies in supercatastrophic regime, as mentioned in the paper. We realize this is not explicitly mentioned in the text and might confuse some readers, we thus added a note to the end of Sec. 3.4.

> Section 4
> - My major concern here is the follow one. The authors are getting parametric
> relations that could be used in collisional models. Form the text in this
> section; I understand that only the new set of simulations (D=10 km) was used
> to derive the parametric relations, but not offer a comparison with the set
> of simulations from Durda et al. (2007) for D=100 km, to test out if these
> follow the same relationship. Just in case, why didnt you consider both
> sets?

> In case both set of simulations were considered to get the parametric
> relations, it should be explicitly said in the text. If it is not included, it
> could be interesting such comparison and discussion.

We thank the referee for this point, as it is also something we left out of our paper. We believe including both sets of simulations would not provide more accurate results. Even if we consider only D_pb=10km simulations, the relevant quantities (slope q, largest remnant M_lr and fragment M_lf) are not well constrained, as seen from Fig. 4 of the paper. Adding one more parameter - the parent body size M_pb - would make ~~it much more difficult to find~~ generic relations fitting all considered data. * We conclude it is better to restrict the dataset and provide more constrained parametric relations. It can be also seen that the D_pb=100km bodies do NOT follow the same relations. This is evident from plots of SFDs in Fig. 1 and E.11-14 - the differences in slopes and largest remnants (fragments) imply we would have to ~~generalize~~ the parametric relation in order to fit both D_pb=10km and D_pb=100km results.

* even more difficult

> - Regarding to the estimations of the SFD slope. Are the authors considering
> the full size range of fragments, or have been excluded the fragments under
> the resolution code? Such consideration could be included in the text.

We only considered the middle part of the SFD, excluding both the largest remnant (if there is one) and the part close to the resolution limit. We did not specify what part of the SFD is used for fitting, so we corrected our mistake by defining the lower and upper cutoff for fitting the power-law, see the beginning of Sec. 4 in the new paper.

> - line 283: Do you mean Q_eff/Q^*_D? On the other hand, concerning to this
> last paragraph, the author mention an interesting point here, which could be
> extended. Is that behaviour related to the fact that the largest remnant
> does not exist?

There should indeed by Q_eff instead of Q, we corrected the typo.

> Appendix A
> - This is an interesting point in order to assess the uncertainty introduced
> by using initial conditions of SPH. I have no complain here, but I am
> wandering how could change the SFD outcomes if you consider lower impact
> energy and on the contrary very high impact energy (supercatastrophic
> events).

The differences between both particle distributions are largest for cratering impacts with a very small impactor. The bigger the impactor, the more similar the SFD is to the SFD of the 'standard' particle grid.

∀ We added a note... ?

> Appendix B
> - line 254: s1, s2, D_0 are no defined along the text.

We thank the referee for another discovered typo, the variables were corrected to q1 and q2.

> - line 358: Do you really mean D=1km and d=22 m? The same in caption figure B.7.

In this appendix, we do indeed use D=1km bodies instead of D=10km. The discussed issues of energy conservations are more prominent in these cases and thus make 1km bodies more suitable for our numerical tests, even though the same issue is present for 10km and also for 100km bodies, although at a negligible level.

> Appendix C
> - line 399, D=1km 10 km??
> Here is a list of less important remarks:
> Line 154 and 171, it is used D_PB however in other cases (i.e. line 172)
> D_pb, please use a uniform notation along the manuscript, check for other
> cases.

> Figures 1: D/ km D (km), also check others figures, most of them have the same typo.
> Figure 2: caption, 2nd line, Do you really mean Fig. D.10 or Figure 1?

Corrected typos.

> Reviewer 2

> Overall this is a straightforward paper presenting results of numerical
> experiments by the first author and collaborators. I have a few comments that
> I hope will improve the presentation of the work.

> My main question concerns the sensitivity of the results to the particular
> values of the Weibull parameters that the authors have chosen. Why did the
> authors choose those particular values for k and m? My understanding is that
> m, in particular, is known to vary over a wide range (m=9 lies in the middle
> of that range, I believe). How sensitive are the results to choices of other
> values for those parameters? In particular, the authors emphasize that their
> results for D=10 km targets are different from the results for previous work
> by Durda et al (2007) with D=100 km targets. (I haven't checked the Durda
> et al 2007 paper, did that paper use the same values for k and m? If so, that
> should be stated, or for that matter, whatever values Durda et al used.)

> Given that the main results of the paper are concerned with the mass,
> velocity, and angular distributions of fragments after impacts, it would
> seem to me that this might be an issue? Have the authors carried out any
> calculations with different values of k and m? I don't know that the authors
> need to carry out a whole suite of calculations with different k and m, but
> some assurance or comparison would be a good thing.

In the original manuscript,
We did not check the dependence on material properties and instead considered them fixed for all performed runs. Selected values are the same as the ones used in Durda at al. 2007; we added a note to Table 1 mentioning this fact. However, it is certainly ~~an~~ important to test the sensitivity of our results to Weibull parameters. To this point, we ran a few simulations for different values of k and m in order to estimate the expected uncertainty Weibull parameters introduce into our results. The tests are described in Appendix B of the new manuscript.

-se additional

> A few other notes: I think it would be good if equations 6-7 were written so
> as to explicitly show the contribution of the artificial viscosity Pi_ij, or
> perhaps its contribution to the pressure P, if that is how it is done.

It is indeed not clear from the text how the artificial viscosity enters the equations; we explicitly ~~added~~ the terms into the equation of motion and energy equation in the resubmitted paper.

> Likewise it would be good to see an explicit expression for the damage D, if
> not in the text, then perhaps in a short appendix.

The equation for evolution of damage D is taken straight from the referenced paper by Benz and Asphaug, 1994. It is quite tricky to correctly discretize the Grady-Kipp damage in SPH (far from a single equation) and it is explained in detail in Sec. 3.2 of Benz and Asphaug, 1994. We would not want to ~~hint~~ the damage discretization is our work, as we use an existing code (SPH5) and the computation of damage was left unchanged. We thus ~~believe~~ the damage discretization ~~does not belong into this section~~.

> Another interesting comparison (in my opinion) would be one between the
> authors' results for fragment mass and velocity distribution and the
> "classical" results for ejecta from cratering impacts into a half-space.
> Given that the authors make a point of discussing their results in the
> "cratering" regime where the impactor diameter is much smaller than the
> target, such a comparison is interesting and appropriate. The classic paper
> for this is Housen et al 1983, J. Geophys. Res. vol. 88, p 2485 but a more
> recent and extensive paper is Housen and Holsapple 2011, Icarus vol. 211, p
> 856. A plot like the log-log plots in Fig 1 of the paper would be
> appropriate. One imagines that the authors' results for the smallest
> impactors would be similar to those from half-space experiments and
> calculations, but is that the case?

The Referee raises an interesting question. The cratering events should indeed produce comparable results to impacts into half-space; experimental data from Housen and Holsapple 2011 could then serve as an independent validation of the ~~used~~ SPH code. We did not attempt to validate the code in our work as we are using already well tested code SPH5 (Benz and Asphaug, 1994, 1995), with ~~but~~ a few modifications*. If we wished to compare cratering impacts with impacts into half-space, the problem setup would also have to be adjusted; currently the impact point and ejected fragments are poorly resolved for cratering events. This Rough discretization does not allow us to compare ejected fragments in detail, for quantitative comparison we would need more SPH particles at the point of impact, possibly using method described in Appendix A of the paper. We can at least say that our results are qualitatively consistent with the impact experiment. Experimental data show that the velocity of ejecta depends on their distance from the point of impact - the ejection velocity decreases with increasing distance - and this is indeed what we see in our simulations. We uploaded one animation of cratering simulation to

http://sirrah.troja.mff.cuni.cz/~sevecek/

Nevertheless, We ~~therefore~~ beg to leave out ~~the~~ comparison from the paper, as it would require ~~major modifications~~. We believe it is a related, but distinct problem - and a good idea for future work in this field.

% vim: set spell spelllang=en fdm=marker:

Finally, let us thank both referees for very interesting and relevant points.